Kremen1 dependence receptor induces SEC24C and ATG9A-dependent autophagic cell death

Sonia Brahim[1,2,*], Thomas Schott[2*], Shiva Ghasemi[1*], Ana Negulescu[2], Clara Geneste[2], Elisabeth Errazuriz-Cerda[3], Gabriel Ichim[1], Patrick Mehlen[2] and Olivier Meurette[1,2,$]

[1]Cancer Cell Death Laboratory, LabEx DEVweCAN, Centre de Recherche en Cancérologie de Lyon, INSERM U1052-CNRS UMR5286, Université de Lyon, Centre Léon Bérard, 69008 Lyon, France.

[2]Apoptosis, Cancer and Development Laboratory- Equipe labellisée 'La Ligue', LabEx DEVweCAN, Centre de Recherche en Cancérologie de Lyon, INSERM U1052-CNRS UMR5286, Université de Lyon, Centre Léon Bérard, 69008 Lyon, France.

[3]Centre d'Imagerie Quantitative Lyon Est, Faculté de Médecine Laënnec, Lyon, France.

[*]Co first authors

Corresponding author: O. Meurette; email: olivier.meurette@lyon.unicancer.fr.

ABSTRACT

Dependence receptors (DRs) induce cell death by apoptosis when unbound by their cognate ligands. Among them, Kremen1 was first described to induce cancer cell death in the absence of its ligand, DKK1. However, the precise mechanism of Kremen1-induced cell death remains unclear. In this study, we demonstrate that Kremen1 induces cell death with autophagic features, contrasting with the apoptotic process typically associated with dependence receptors. Specifically, the pharmacological inhibition of autophagy, or genetic silencing of key autophagy effectors, efficiently suppresses this cell death process. A biotin proximity labeling for protein-protein interactions identified SEC24C, a component of the COP-II complex, as a critical effector in Kremen1-induced autophagy and cell death. Our findings further reveal that Kremen1 is in proximity with SEC24C and ATG9A after vesicular trafficking and fosters the interaction of SEC24C with ATG8, ERGIC and ATG9A. This potentially underlies the increased number of autophagosomes leading to cell death. The induction of aberrant autophagy by Kremen1 deserves particular attention, especially as the Kremen1/DKK1 pair is frequently altered in cancers. Thus, targeting this pathway may offer a potential strategy for treating cancers resistant to current therapies.

Keywords: Cancer, Cell death, ATG9A, SEC-24C, Dependence Receptors

51

52 **ABBREVIATIONS**

53

54 APEX: Ascorbate Peroxidase

55 ATG: Autophagy related genes

56 CNS: Central Nervous System

57 COP-II: Coat Protein Complex II

58 DKK1: Dickkopf-Wnt Signaling Pathway Inhibitor

59 DR: Dependence Receptor

60 ERGIC: ER-Golgi intermediate compartment

61 LRP5/6: LDL Receptor Related Protein 5

62 PLA: Proximity Ligation assay

63 STING: Stimulator Of Interferon Response CGAMP Interactor

64 TCGA: The Cancer Genome Atlas

65 WNT: Wingless-related integration site

66

67

68

69

70

71

72

INTRODUCTION

Dependence receptors (DR) form a family of transmembrane receptor proteins crucial in maintaining cellular homeostasis. Notably, they play a significant role in cancer progression by regulating cell proliferation when bound to their ligand, and by inducing apoptosis in absence of their ligand [1]. Despite their structural diversity, these receptors constitute a functional family, each shown to induce apoptosis through different mechanisms [2–4]. Kremen1, a recently identified DR, has been recognized for its ability to induce cell death in absence of its ligand, Dickkopf-Wnt Signaling Pathway Inhibitor (DKK1)[5]. Initially characterized as a Wnt signaling inhibitor, Kremen1/2 serves as a high-affinity receptor for DKK1. Together, they cooperate to recruit the WNT co-receptor LRP5/6, thereby inhibiting the Wnt/β-catenin pathway [6]. Further studies suggested that Kremen1/2 are not directly involved in this inhibition but they recruit DKK1 and present it to LRP5/6 when the WNT coreceptor is in excess [7]. Once the ternary complex between DKK1, Kremen1/2, and LRP5/6 is formed, it undergoes rapid clathrin-mediated endocytosis, thereby limiting the number of available Wnt co-receptors on the plasma membrane [8,9]. Kremen1/2 has been implicated in essential developmental processes, including anteroposterior patterning of the central nervous system (CNS) in *Xenopus* [10], as well as DKK1 in mice [11]. Kremen1 has also more recently been described as a receptor for enteroviruses [12]. Similar to other dependence receptors, the Kremen1/DKK1 receptor-ligand pair may play a significant role in regulating cancer initiation and progression. Kremen1 expression is frequently lost in various cancers, including glioblastoma, neuroblastoma, lung cancer, kidney cancer, stomach cancer, melanoma, and lymphoma [13]. Conversely, its ligand DKK1 is upregulated in several primary tumor type and is elevated in the serum of cancer patients [14]. Furthermore, high serum levels of DKK1 are associated with poor prognosis in breast, prostate and bladder cancers [15–17], as its overexpression similarly correlated with poor outcomes in hepatocellular carcinoma [18]. The cell death function of Kremen1 in absence of DKK1 may therefore be implicated in cancer progression. Dependence receptors have been shown to induce apoptotic cell death. However, the mechanism by which Kremen1 induces cell death has not been characterized. We bring here novel insight on this cell death pathway, demonstrating that differently from other dependence receptors Kremen1 is inducing autophagy-dependent cell death in breast and pancreatic cancer cells. This is of particular

103 significance as apoptosis induction may not always be a good strategy in cancer treatment [19]. We
104 further describe a mechanism involving SEC24C and ATG9A interacting with Kremen1 after its
105 membrane trafficking that fosters their interaction with ATG8, increasing autophagosomes
106 biogenesis.

107

RESULTS

The expression of both Kremen1 and DKK1 pair is frequently altered in cancer

Given the established role of DR and their ligands in tumor suppression, we first examined the expression profiles of the Kremen1/DKK1 pair across various datasets. Consistent with characteristics of tumor suppressors, Kremen1 expression was reduced in multiple cancer types, including breast cancer, colon cancer, and head and neck cancers (Figure 1A). In contrast, DKK1 expression was markedly upregulated across several cancers (Figure 1B). Consistently, analysis of The Cancer Genome Atlas (TCGA) dataset showed that patients with high DKK1 expression had worse overall survival in pancreatic ductal adenocarcinoma and in breast cancers (Figure 1C-D). Interestingly, DKK1 expression is higher in basal-like (TCGA data) and HER2-overexpressing breast cancers (Figure 1E), an observation corroborated in the METABRIC dataset, where DKK1 was elevated in HER2+ and HER2-/ER- subtypes (Figure 1F). In contrast, Kremen1 expression did not vary significantly by subtype in the TCGA dataset, except for a significant difference between luminal B and HER2-enriched (Figure 1G), and a slight but significantly increase in HER2+ cases in the METABRIC dataset (Figure 1H). These findings suggest that alterations in the Kremen1/DKK1 pair may be particularly relevant in basal-like (ER-/HER2-) breast cancers, where *dkk1* gene expression is high while *Kremen1* expression is low. Consequently, we decided to focus on triple-negative breast cancers for further investigation. We also studied pancreatic cell lines given the predictive value of DKK1 in PDAC. Given Kremen1's role in Wnt inhibition in the presence of DKK1, we examined whether Wnt gene signatures were altered in patients with high Kremen1/DKK1 expression, but observed no significant differences meaning the expression of DKK1 and Kremen1 is not associated to Wnt signature (Figure 1I). Thus, the deregulated Kremen1/DKK1 expression ratio favoring DKK1 is a potential biomarker of poor prognosis.

Kremen1-induced cell death lacks classical apoptotic features

Kremen1 has previously been described as a DR inducing features of apoptotic cell death[5]. In order to investigate the mechanisms underlying Kremen1-induced cell death, we developed several stable cell lines expressing Kremen1 upon doxycycline treatment. Kremen1 was induced in a time and dose dependent manner (supplementary figure 1A). Furthermore, whereas

doxycycline treatment had no impact on cell death (supplementary Figure 1B), Kremen1 induction was followed by a significant increase of cell death: up to 50% in MDAMB231 cells, 30% in HEK293 and 20-30% in BxPC3 (supplementary figure 1C-E), showing that Kremen1-induced pathway is conserved across different cell types. We further focused on MDAMB231 and BXPC3, as model of breast cancer and pancreatic cancer and used IncuCyte Imager-based live cell imaging to monitor cell death every 2 hours upon a long period of time. We observed both in MDAMB231 and BxPC3 accumulation of cell death upon Kremen1 induction from 24 up to 60 hours following Kremen1 induction (Figure 2A, supplementary Figure 1F). Additionally, long-term clonogenic survival revealed a reduction in colony formation upon Kremen1 induction (Figure 2B). Co-expression of DKK1 reduced Kremen1-induced cell death, supporting the previously documented DR activity of Kremen1 (Figure 2C). Furthermore, siRNA targeting DKK1 also induced cell death although to a lower extend than Kremen1 induction (Supplementary Figure 1G). Kremen1 expression led to activation of caspase-3, which was efficiently inhibited by treatment with Q-VD-OPh pan-caspase inhibitor (supplementary Figure 2A). However, treatment with Q-VD-OPh (QVD) inhibited only very partially cell death in MDAMB231 (Figure 2D) and had no effect in HEK293 cells either (Supplementary figure 1D). We also treated cells with additional caspase inhibitors, including IETD and DEVD, and observed no impact on cell death, indicating that these caspases are not involved in our cell death model (data not shown). Interestingly, treatment of Kremen1-expressing cells with ABT263 triggered a rapid shift towards apoptotic features, indicating that these cells remain responsive to apoptotic stimuli and that Kremen1-induced caspase activity may prime cells to a stronger apoptotic stimulus (Supplementary Figure 2B). We further characterized cell morphology by Nanolive microscope-based holotomography imaging of cells expressing Kremen1 and of cells treated with an apoptosis inducer as a control (BV6). Cells treated with BV6 exhibited membrane blebbing and cell contraction, while Kremen1-overexpressing cells displayed a phenotype characterized by cellular swelling (Figure 2E). Treating cells with necrostatin-1 or ferrostatin did not rescue cell death induction showing that Kremen1 is not inducing necroptosis or ferroptosis (Figure 2F and supplementary figure 2C). Thus, our results indicate that kremen1 induces a form of cell death distinct from classical forms of programmed cell death.

168

169 **Kremen1 induced-cell death displays autophagic features**

170 Prior to examining the specific mechanisms of Kremen1-induced cell death, we analyzed
171 the morphology of dying cells using transmission electron microscopy (TEM). We did not observe
172 apoptotic features like membrane blebbing or nuclear condensation and cells appeared to increase
173 in volume rather than exhibit the typical apoptotic shrinkage (Figure 3A). Across multiple time
174 points, in both adherent and non-adherent cells, the dying cells consistently displayed autophagic
175 features, including an accumulation of vacuoles, phagophores, autophagosomes, and multilamellar
176 bodies (supplementary figure 3A). In the supernatant, rare apoptotic cells were observed although
177 most of dead cells appeared necrotic (Supplementary figure 3B). We confirmed autophagy
178 induction through molecular analyses, evidenced by the accumulation of the lipidated form of LC3
179 and a decrease in p62 expression upon Kremen1 induction, as shown by western blotting (Figure
180 3B), and the formation of dense LC3 puncta in immunofluorescence assays (Supplementary Figure
181 4A,B) indicating that autophagosomes are increased in dying cells both in MDA-MB231 and
182 BxPC3 cells. Moreover, no LC3 lipidation was observed in control cells treated with doxycycline
183 (Supplementary figure 4C). In agreement with autophagy being regulated by the DR function of
184 Kremen1, siRNA targeting DKK1 induced autophagic features as does Kremen1 expression
185 (supplementary figure 4D). We next characterized autophagic flux by expressing Kremen1 in cells
186 expressing the RFP-GFP-LC3 reporter construct. We observed accumulation of RFP-only LC3 dots
187 upon Kremen1 induction demonstrated an induction of the autophagic flux and not a mere
188 inhibition of late autophagic phase leading to accumulation of autophagosomes (Figure 3C).

189 **The autophagic machinery is indispensable for Kremen1-induced cell death.**

190 We next sought to assess the requirement of the autophagic machinery in the observed cell
191 death. Spautin as well as wortmanin treatment which inhibit the early stage of autophagic flux by
192 preventing autophagosome formation, resulted in a significant decrease in cell death and LC3
193 lipidation (Figure 3 D,E, supplementary figure 5A,B). In contrast, treatment with Bafilomycin-A
194 and Chloroquine, which both block the flux at late stages inducing autophagosome accumulation
195 led to an increase of cell death following kremen1 expression (Supplementary Figure 5C). This
196 suggests that the presence of autophagosomes or certain autophagic components may be essential

197 for cell death induction. While autophagy is often induced following apoptosis as a mechanism
198 thought to inhibit cell death, in our model, treatment with Spautin1 completely blocked cell death
199 by inhibiting LC3 lipidation (Figure 3D, supplementary Figure 5B) without affecting caspase
200 activation (Supplementary figure 5D). Furthermore, knock-out of APAF1 which inhibits caspase
201 activation had no effect on cell death nor on LC3 lipidation (supplementary Figure 5E-G),
202 suggesting that caspase activation in not involved in autophagy induction in this context.
203 Surprisingly, knock-down of ATG5 by siRNA or by CRISPR knock-down had no impact on cell
204 death induction nor on caspases activation (data not shown) demonstrating the involvement of
205 atypical autophagy. As ATG5 was not involved in Kremen1-induced cell death, we examined the
206 role of ATG9A, since it is a protein which facilitates membrane recruitment and autophagosome
207 membrane expansion [20]. We further showed that inhibition of ATG9 via siRNA (supplementary
208 Figure 6A) significantly reduced cell death in both MDA-MB-231 and BxPC3 cell lines,
209 highlighting its essential role in this process (Figure 3F-G). We also investigated the involvement
210 of ATG18 since they have shown to participate with ATG9A to autophagosome membrane
211 expansion [21]. siRNA mediated knock-down of ATG18B also partially rescued Kremen1-induced
212 cell death (Figure 3H). Altogether, these findings support the involvement of an atypical form of
213 autophagy relying on ATG9A and ATG18B to induce aberrant accumulation of autophagosomes
214 leading to autophagic cell death.

215

216 **SEC-24C is involved in Kremen1-induced cell death**

217

218 To elucidate the mechanisms underlying this autophagy-mediated cell death, we analyzed
219 the Kremen1 interactome via mass spectrometry. For this purpose, we employed a biotin proximity
220 labeling for protein-protein interactions proximity labeling approach by fusing Kremen1 with an
221 ascorbate peroxidase (APEX2) enzyme to perform enzyme-mediated biotin identification. Using
222 the same doxycycline-inducible system, we expressed a Kremen1-APEX fusion protein to identify
223 proteins in close proximity. We first confirmed that the Kremen1-APEX fusion did not alter
224 Kremen1-mediated signaling, and induced autophagy and cell death with comparable efficiency to
225 Kremen1 alone (data not shown). We then used streptavidin beads to isolate proteins proximal to
226 Kremen1-APEX, followed by mass spectrometry analysis, which yielded a list of proteins most
227 enriched upon doxycycline addition and subsequent Kremen1 induction (Figure 4A,B). Among the

most enriched proteins were SEC24C and other proteins of the COP-II complex. Two major clusters appeared using String-database analysis (Figure 4B). The first one was enriched in membrane-associated, adhesion and focal adhesion proteins such as integrins (ITGB1, ITGA6, ITGA2), taline (TLN1), vinculin (VCL), paxillin (PXN), showing the membrane localization of Kremen1 in the experiments. The second cluster was a cluster of COP-II complex proteins, including SEC23A and B, SEC24 B and C as well as SEC31A. This complex particularly caught our attention since the COP-II complex has been implicated in atypical autophagy regulation [22,23]. Specifically, SEC24C stands out due to its role in autophagy regulation by its interaction with ATG9 to increase autophagosomes abundance in yeast and is implicated in STING-induced autophagy and cell death [24,25]. Immunofluorescence analysis confirmed partial interaction between Kremen1 and SEC24C (Figure 4C). To investigate the potential role of SEC24C during Kremen1 cell death induction, we inhibited its expression via siRNA and found a significant reduction of Kremen1-induced cell death in both MDA-MB-231 and BxPC3 cell lines (Figure 4D). Furthermore, knocking-down of SEC24C induced a significant reduction of LC3 lipidation upon Kremen1 induction (Figure 4E). Altogether these data demonstrate that SEC24C is involved in Kremen1-induced autophagy and cell death.

Kremen1 is at proximity of SEC24C and ATG9 after being internalization.

As SEC24C and the COPII complex are involved in protein trafficking, we further wanted to characterize the localization of SEC24C and ATG9 at proximity of Kremen1 after membrane trafficking. We set up Proximity labelling assay (PLA) by using Kremen1/SEC24C and Kremen1/ATG9A antibodies and could observe significant co-localization of Kremen1 with ATG9A and SEC24C spread in the cytoplasm (Figure 5A). Furthermore, DKK1 expression together with Kremen1 induces a reduction of Kremen1 interaction with ATG9A (Supplementary figure 6B), suggesting that Kremen1 has to be addressed to the membrane to further interact with ATG9A. To test this hypothesis, we performed pulse chase experiment by adding Kremen1 antibody on live, non-permeabilized cells and performed PLA with adding ATG9A or SEC24C antibodies after different time points. By this technique we visualize the proximity of internalized Kremen1 (iK1) with intracellular SEC24C or ATG9A. We could demonstrate a time dependent increase in PLA signals for internalized Kremen1/SEC24C and internalized Kremen1/ATG9A. Altogether, these experiments show that localization of Kremen1 with SEC24C and ATG9A is at

259 least in part dependent on Kremen1 addressing to the membrane and is dependent on DKK1.

260

261 **Kremen1 induces recruitment of ATG8 at ERGIC (LMAN1) together with SEC24C and**
262 **ATG9A**

263 As we observed that SEC24C was involved in Kremen1 induced autophagy, we then sought to
264 determine whether SEC24C was associated with autophagosomes upon Kremen1-dependent cell
265 death induction. To this end, we performed immunoprecipitation of SEC24C in the presence and
266 absence of Kremen1 and observed that, upon Kremen1 induction, SEC24C interacted with ATG8,
267 indicating that SEC24C plays a specific role in autophagy regulation within this autophagic cell
268 death pathway (Figure 6A). This observation was further validated through confocal microscopy,
269 which revealed a partial colocalization of ATG8 and SEC24C in BxPC3 cells in condition of
270 Kremen1 expression, as indicated by yellow puncta (Figure 6B). We next demonstrated that upon
271 Kremen1 induction, ATG8 localization at ERGIC (LMAN1) together with SEC24C and ATG9
272 was increased (Figure 6C). Altogether, these findings demonstrate that SEC24C and ATG9 are
273 essential components in mediating Kremen1-induced cell death by increasing autophagosome
274 biogenesis.

275

276

277

DISCUSSION

Kremen1, initially identified as a receptor involved in DKK1-mediated Wnt signaling inhibition [6], was later characterized as a DR [5]. DRs constitute a diverse family of structurally unrelated receptors that share the unique capacity to actively induce cell death in the absence of their respective ligands. Until now, all known DRs have been shown to induce apoptosis through distinct pathways that ultimately converge to caspase-3 activation [26]. In the case of Kremen1, Causeret et al. reported that its overexpression led to caspase-3 cleavage, consistent with an apoptotic pathway similar to that of other DRs, but without any characterization of the cell death signaling pathway. In this study, we confirmed that Kremen1 expression induces caspase-3 activation despite the absence of classical apoptotic features, as evidenced by transmission electron microscopy and time-lapse tomographic microscopy. Moreover, inhibition of caspase activity with qVD-Oph had very little effect on cell death indicating that effector caspases are dispensable for Kremen-1 induced cell death. It is plausible to consider that caspase activation in this context occurs as a bystander event, insufficient to directly induce cell death but potentially involved in non-apoptotic roles as it already has been shown before [27]. Another explanation would be that the aberrant increase of autophagosomes may prevent the cleavage of canonical substrates necessary for apoptotic progression. However, cells expressing Kremen1 remain responsive to apoptotic stimuli, particularly in the early stages following Kremen1 induction, as treatment with ABT263, a Bcl-xL and Bcl-2 antagonist, rapidly induces canonical apoptosis indicating that cells remain sensitive to apoptotic stimuli.

Instead of apoptotic features, we consistently observed autophagic features in dying cells. Cells exhibiting autophagic features have long been reported in physiological cell death [28]. However, the presence of abundant autophagosomes in dying cells does not necessarily imply that autophagy is the direct trigger of cell death. Autophagy is well-established as a survival pathway under nutrient-limiting conditions [29] and it is generally considered to limit apoptosis and confer resistance to cell death [30]. Evidence from physiological development supports the role of autophagy as a *bona fide* cell death mechanism. In Drosophila, for example, autophagy, not apoptosis, is essential for programmed cell death in the midgut [31] and is also required for the degradation of salivary gland cells [32]. Additionally, autophagy-dependent cell death, termed autosis, can be induced by autophagy-stimulating peptides, such as Tat-Beclin1, which holds potential for therapeutic applications [33]. The cell death observed following Kremen1 induction displays

310 phenotypic similarities with Tat-Beclin1-induced autosis. However, treatment with Na^+/K^+
311 inhibitors did not rescue this cell death (data not shown), suggesting mechanistic differences from
312 canonical autosis. Kremen1-induced cell death results in a substantial accumulation of
313 autophagosomes, which may contribute to the observed cytotoxicity. Autophagosome
314 accumulation alone has been reported as sufficient to induce cytotoxic effects [34] and the timing of
315 autophagosome accumulation relative to ATP availability and lysosomal homeostasis may be a
316 critical factors [35]. Although protein overexpression may induce cellular stress triggering autophagy,
317 the phenotype observed with Kremen1 has never been observed with other DRs using the same
318 induction strategy [3]. Furthermore, DKK1 addition is reducing cell death in conditions in which
319 Kremen1 expression is induced at the same levels (Figure 1C). By a proximity biotin ligation assay,
320 we identified enrichment of members of the COP-II complex associated with Kremen1 (Figure 4).
321 The COP-II complex primarily serves two functions: it facilitates the physical deformation of the
322 endoplasmic reticulum membrane into vesicles and selects cargo molecules for transport to the
323 Golgi apparatus. Interestingly, COP II vesicle are diverted to autophagosome formation in response
324 to stresses [36,37]. Furthermore, different members of this complex have been shown to be involved
325 in autophagosomes formation [38–40]. More specifically, SEC24C, identified as the most enriched
326 component of the COPII complex within the Kremen1 interactome, functions as a pivotal effector
327 in autophagic process, including ER-Phagy [22] as well as STING-associated autophagy and cell
328 death [24,41]. Furthermore, under cellular stress, such as nutrient deprivation, SEC24C undergoes
329 phosphorylation by the kinase Hrr25, enabling it to interact with ATG9 [38]. Experimental evidences
330 demonstrate that SEC24C and ATG9A are implicated in Kremen1-mediated induction of
331 autophagic cell death. Pulse-chase labeling analyses have further revealed colocalization of
332 Kremen1 with both ATG9A and SEC24C following membrane trafficking. This interaction
333 facilitates LC3 redistribution to ATG9A, the ER-Golgi intermediate compartment (ERGIC) and
334 SEC24C illuminating previously uncharacterized aspects of the Kremen1-initiated signaling
335 cascade. Unlike other DRs Kremen1 orchestrates a unique cell death modality centered on the
336 autophagic machinery. We also showed that in presence of its ligands DKK1, Kremen1 is not or
337 much less interacting with ATG9A. We therefore hypothesize that upon Kremen1 induction or
338 limitation for DKK1 ligand, Kremen1 is recruiting ATG9A vesicle to SEC24C/ATG8 site of
339 autophagosome formation creating an increased demand for membrane resources to support
340 autophagosome formation.

Given the relevance of DRs as therapeutic targets in cancer [26], we examined the status of the Kremen1/DKK1 pair across various cancer types. Our observations indicate that Kremen1 expression is frequently downregulated in multiple cancers, suggesting a potential role for Kremen1 as a tumor suppressor through its autophagy-dependent cell death pathway. Notably Sato et al [14] reported elevated DKK1 serum levels in patients, stronger than those observed here in RNA sequencing data. In breast cancer specifically, while some patients exhibited high DKK1 levels, the median expression of DKK1 in matched tumor/normal samples remained below 1 in breast tumors (Figure 1B), contrasting with the significant serum increases observed by Sato et al,. Additionally, DKK1 expression has been linked to metastasis and poor survival outcomes in lymph node-positive breast cancer patients [42]. Notably, recent studies have demonstrated that autophagic cell death may contribute to tumor suppression by limiting chromosomal instability [43,44]. We are currently exploring the therapeutic potential of activating this novel autophagic cell death pathway as a targeted approach in cancer treatment.

356
357 **EXPERIMENTAL PROCEDURES**

358 **Plasmids construction**

359 The inducible Sleeping Beauty transposon system was used as backbone for cloning the murin
360 Kremen1 gene under doxycycline inducible control. The Kremen1 gene was fused in N-terminal
361 with an HA tag. Two constructs were realized: pitr1-Kremen1, containing a GFP insertion
362 constitutively expressed and a puromycin resistant gene constitutively expressed and pitr2-
363 Kremen1 containing a RFP insertion and a zeocin resistant gene both constitutively expressed.

364 **Cell culture**

365 Human breast cancer cell line MDA-MB231 and human embryonic kidney HEK293T cells were
366 obtained from ATCC (UK) and maintained in Dulbecco's Modified Eagle's Medium (DMEM)
367 supplemented with 10% fetal bovine serum (FBS) and 1% penicillin/streptomycin.

368 For the establishment of stable cell lines MDA-MB231 and HEK293T with pitr1-Kremen1 or pitr2-
369 Kremen1, the cells were transfected with 1,6 µg plasmid, 0,4 µg SB100x transposase and Fugen
370 (Promega) in a ratio total DNA : transfectant of 1:3 and then selected with puromycin (Gibco Life
371 Technologies) or zeocin (Invitrogen) for 2 to 4 weeks. MDA-MB231 clones were selected by flow
372 cytometry in accordance with high or low expression of GFP.

373 For inhibitor treatments cells were incubated with 20 µM q-VD (Sigma-Aldrich SML0063), 40 µM
374 Necrostatin-1 (Sigma-Aldrich N9037), 5 mM 3-MethylAdenin (Sigma-Aldrich M9281) in
375 different combinations. For induction of Kremen1, Doxycycline (Sigma-Alderich) was added in
376 various concentrations in cell media.

377 siRNA transfections were realized in 6-well plates with 10nM siRNA and 3µl Lipofectamine
378 RNAiMAX (Life) according to the manufacturer instructions. The siRNA used were Life Silencer
379 Select Negative control #1 Cat#4390843, lot AS021N56;

380

381

382 **Transmission electron microscopy (TEM)**

383 Cells were prepared for fixation in 6-well plates or in supernatants with 1 volume complete DMEM
384 medium/1 volume glutaraldehyde 4% for 15 minutes at 4°C. Cells were fixed in 1 volume
385 cacodylate pH 7,4/1volume g glutaraldehyde 4%. Attached cells were harvested by scratching and
386 centrifugated. The sample were washed three times in saccharose 0.4 M/0.2 M Na C-HCl-
387 Cacodylate-HCl pH 7.4 à 0,2 M for 1 hour at 4°C, and postfixed with 2% OsO4/0.3 M Na C-
388 HCl Cacodylate-HCl pH 7.4 1hour at 4°C. Then cells were dehydrated with an increasing ethanol
389 gradient (5minutes in 30%, 50%, 70%, 95% and 3 times for 10 minutes in absolute ethanol.
390 Impregnation was performed with Epon A (50%) plus Epon B (50%) plus DMP30 (1,7%).
391 Inclusion was obtained by polymerisation at 60°C for 72hrs. Ultrathin sections (approximately 70
392 nm thick) were cut on a ultracut UC7 (Leica) ultramicrotome, mounted on 200 mesh copper grids
393 coated with 1:1000 polylisine, and stabilized for 1day at room temperature (RT) and, contrasted
394 with uranyl acetate and lead citrate. Sections were examined with a Jeol 1400 JEM (Tokyo,Japan)
395 transmission electron microscope equipped with a Orius 600 camera and Digital Micrograph.

396 **Caspase-3 activity assay**

397 Cells were harvested by trypsinization and cell pellets were obtained by centrifugation at 4°C and
398 lysed. The caspase-3 activity assay was performed according to the manufacturer's instructions
399 (Biovision caspase-3 colorimetric assay kit). Total protein concentrations were measured with the
400 BCA assay kit using BSA as a standard (Pierce Biotechnology, Rockford, IL, USA). Absorbance
401 readings were done on a TECAN infinite F500.

402 **PI/Sytoxgreen stained cells counting**

403 Cells were plated in 96-well plates, incubated with 0,33 ng/ml PI or Sytoxgreen and different
404 treatments. The plates were further monitored by Incucyte Zoom (Essenbio) for several days. The
405 PI positive cells were normalized by the confluence percentage for each well, at several time points.

406 **Immunofluorescence staining**

407 Fixation and staining were performed simultaneously. Attached cells samples were fixed with
408 freshly prepared 4% PFA, washed 3 times with PBS for 5 minutes and permeabilized with PBS-

409 0.2% Triton X-100 (TX-100) for 10 minutes at room temperature. Samples were then washed 3
410 times with PBS for 5 minutes and blocked in PBS with 4% bovine serum albumin (BSA), 2%
411 normal donkey serum and 0.2% TX-100 for one hour. Primary antibodies were diluted in the
412 blocking solution at a dilution of 1:200 for the anti-Kremen1 produced antibodies and 1:50 for anti-
413 HA (Sigma-Aldrich H4908). Alexa-conjugated secondary antibodies (Alexa555-donkey anti
414 rabbit, Alexa488-donkey anti rabbit, Alexa488-donkey anti mouse) were used at 1:1000 dilution.
415 1 µg/ml DAPI was added at the end to stain nuclei. Images were acquired with Zeiss Axio
416 fluorescence microscopy.

417 **Quantitative RT PCR**

418 mRNAs were extracted with the NucleoSpin RNA kit (Machery-Nagel) according to
419 manufacturer's instructions. cDNAs were generated with the iScript cDNA Synthesis kit (BIO-
420 RAD) according to the manufacturer's instructions. Real-time quantitative RT-PCR was performed
421 using a LightCycler 480 (Roche Applied Science).

422 **Western Blot**

423 Cells were lysed in SDS buffer (2% SDS, 150mM NaCl, 50mM Tris-HCl, pH 7.4), denaturated at
424 94℃ for 5 minutes. Protein concentration was measured with the BCA assay kit using BSA as a
425 standard (Pierce Biotechnology, Rockford, IL, USA) according to manufacturer's instructions. The
426 primary antibodies used were : anti-HA (1:1000 dilution, Sigma-Aldrich H4908), anti-LC3 (1:1000
427 dilution, Cell signaling) and an anti-actin conjugated with HRP ().

428 **Proximity-Dependent Biotinylation assay**
429
430 In order to identify new partners of the Kremen1 induced signalization, a proximity
431 biotinylation screening of the receptor Kremen1 was performed. The receptor Kremen1 was fused
432 to the soybean ascorbate peroxydase (APEX2) in a Tet–ON/OFF plasmid (PITR). MDA-MB 231
433 cell line was stably transfected with the PITR Kremen1-APEX plasmid expressing the receptor
434 fused to APEX under DOX treatment. For each biotinylation experiment 30 million cells were
435 seeded. 2 conditions were chosen, a control condition without induction of Kremen1 (DOX 0) and
436 the dox treated condition (DOX 0.25). DOX (0.25 µg/mL) was added 24 hours after seeding and
437 biotinylation was performed after 24 hours of treatment. 500 µm Biotin Phenol (BP) in DMEM
438 and incubated for 30 minutes at 37°C. Fresh diluted H_2O_2 was then directly added in BP/DMEM at

439 a concentration of 1 mM for 1 minute. After 1 minute, the supernatant was collected and 15 mL of
440 a quenching solution (10 mM sodium ascorbate – 5 mM Trolox – 10 mM sodium azide solution)
441 was added to the dish to stop the biotinylation reaction.
442
443 Three washing steps were repeated in 20 mL quenching solution. Between each washing step, cells
444 were centrifugated for 4 minutes. The quenching solution was then discarded. A centrifugation for
445 10 minutes was then performed. The quenching solution was aspirated and the dry pellet was lysed.
446 RIPA lysis buffer supplemented with 1X protease inhibitor cocktail and with quencher at 1X was
447 used. RIPA lysis buffer was made in a total volume of 50 mL, containing: 12.5 mL Tris Hcl (250
448 mM), 7.5 mL NaCl (750 mM), 1.25 mL SDS 20% (0.5% final), 12.5 mL NaDeoxy 10% (2.5%
449 final),2.5 mL NP40 (5% final) and 13.75 mL H2O. For each condition, 500µL of lysis buffer was
450 used. Samples were vortexed to facilitate lysis. Protein concentration was measured with Pierce
451 660nm protein assay kit (ThermoFicher scientific). 2 mg of proteins was used for enrichment on
452 100µL of streptavidin magnetic beads (ROCHE, ref 11641786001) at +4°C for 2 hours. The
453 supernatant was then discarded and beads washed at 4°C for 5 minutes twice with RIPA buffer,
454 once with KCl (1M), once with Na_2CO_3 (0.1M) and twice Urea (2M) in Tris HCl 10 mM at pH 8.0.
455
456 Proteins were then eluted for 10 minutes at 95°C in a protein loading buffer supplemented with
457 biotin (2 mM) and DTT (20 mM). Samples were then quickly vortexed and cooled on ice for 5-10
458 minutes. Beads were then pelleted using a magnetic rack, frozen at -80°C and sent to the mass
459 spectrometry (MS) platform EDyP in Grenoble on dry ice.
460

461 **Statistical analysis**

462 If samples followed a Gaussian distribution, one-way ANOVA or two-way ANOVA were applied,
463 either paired-ratio or unpaired depending on the experimental data. When samples did not pass the
464 normality test, non-parametric test was applied (Mann-Whitney for unpaired samples and
465 Wilcoxon signed-rank test for paired samples). * : $p<0,05$; ** : $p<0,01$; *** : $p<0,001$.

466

467

468 **REFERENCES**

469 1. Negulescu A, Mehlen P. Dependence receptors – the dark side awakens. FEBS J 2018;
470 285:3909–24.
471 2. Ichim G, Genevois A-L, Ménard M, Yu L-Y, Coelho-Aguiar JM, Llambi F, Jarrosson-
472 Wuilleme L, Lefebvre J, Tulasne D, Dupin E, et al. The Dependence Receptor TrkC Triggers
473 Mitochondria-Dependent Apoptosis upon Cobra-1 Recruitment. Molecular Cell 2013; 51:632–
474 46.
475 3. Wang H, Boussouar A, Mazelin L, Tauszig-Delamasure S, Sun Y, Goldschneider D,
476 Paradisi A, Mehlen P. The Proto-oncogene c-Kit Inhibits Tumor Growth by Behaving as a
477 Dependence Receptor. Molecular Cell 2018; 72:413-425.e5.
478 4. Fombonne J, Bissey P-A, Guix C, Sadoul R, Thibert C, Mehlen P. Patched dependence
479 receptor triggers apoptosis through ubiquitination of caspase-9. Proc Natl Acad Sci USA 2012;
480 109:10510–5.
481 5. Causeret F, Sumia I, Pierani A. Kremen1 and Dickkopf1 control cell survival in a Wnt-
482 independent manner. Cell death and differentiation 2016; 23:323–32.
483 6. Mao B, Wu W, Davidson G, Marhold J, Li M, Mechler BM, Delius H, Hoppe D, Stannek
484 P, Walter C, et al. Kremen proteins are Dickkopf receptors that regulate Wnt/beta-catenin
485 signalling. Nature 2002; 417:664–7.
486 7. Wang K, Zhang Y, Li X, Chen L, Wang H, Wu J, Zheng J, Wu D. Characterization of the
487 Kremen-binding site on Dkk1 and elucidation of the role of Kremen in Dkk-mediated Wnt
488 antagonism. The Journal of biological chemistry 2008; 283:23371–5.
489 8. Mishra SK, Funair L, Cressley A, Gittes GK, Burns RC. High-affinity Dkk1 receptor
490 Kremen1 is internalized by clathrin-mediated endocytosis. PloS one 2012; 7:e52190.
491 9. Yamamoto H, Sakane H, Yamamoto H, Michiue T, Kikuchi A. Wnt3a and Dkk1 regulate
492 distinct internalization pathways of LRP6 to tune the activation of beta-catenin signaling.
493 Developmental cell 2008; 15:37–48.
494 10. Davidson G, Mao B, del Barco Barrantes I, Niehrs C. Kremen proteins interact with
495 Dickkopf1 to regulate anteroposterior CNS patterning. Development 2002; 129:5587–96.
496 11. Mukhopadhyay M, Shtrom S, Rodriguez-Esteban C, Chen L, Tsukui T, Gomer L,
497 Dorward DW, Glinka A, Grinberg A, Huang SP, et al. Dickkopf1 is required for embryonic head
498 induction and limb morphogenesis in the mouse. Developmental cell 2001; 1:423–34.
499 12. Staring J, Van Den Hengel LG, Raaben M, Blomen VA, Carette JE, Brummelkamp TR.
500 KREMEN1 Is a Host Entry Receptor for a Major Group of Enteroviruses. Cell Host & Microbe
501 2018; 23:636-643.e5.
502 13. Nakamura T, Nakamura T, Matsumoto K. The functions and possible significance of
503 Kremen as the gatekeeper of Wnt signalling in development and pathology. Journal of cellular
504 and molecular medicine 2008; 12:391–408.
505 14. Sato N, Yamabuki T, Takano A, Koinuma J, Aragaki M, Masuda K, Ishikawa N, Kohno
506 N, Ito H, Miyamoto M, et al. Wnt inhibitor Dickkopf-1 as a target for passive cancer
507 immunotherapy. Cancer research 2010; 70:5326–36.
508 15. Rachner TD, Thiele S, Gobel A, Browne A, Fuessel S, Erdmann K, Wirth MP, Frohner
509 M, Todenhofer T, Muders MH, et al. High serum levels of Dickkopf-1 are associated with a poor
510 prognosis in prostate cancer patients. BMC cancer 2014; 14:649.
511 16. Sun DK, Wang L, Wang JM, Zhang P. Serum Dickkopf-1 levels as a clinical and
512 prognostic factor in patients with bladder cancer. Genetics and molecular research : GMR 2015;

513 14:18181–7.
514 17. Zhou SJ, Zhuo SR, Yang XQ, Qin CX, Wang ZL. Serum Dickkopf-1 expression level
515 positively correlates with a poor prognosis in breast cancer. Diagnostic pathology 2014; 9:161.
516 18. Huang Y, Yang X, Zhao F, Shen Q, Wang Z, Lv X, Hu B, Yu B, Fan J, Qin W.
517 Overexpression of Dickkopf-1 predicts poor prognosis for patients with hepatocellular carcinoma
518 after orthotopic liver transplantation by promoting cancer metastasis and recurrence. Medical
519 oncology 2014; 31:966.
520 19. Castillo Ferrer C, Berthenet K, Ichim G. Apoptosis – Fueling the oncogenic fire. FEBS J
521 2021; 288:4445–63.
522 20. Holzer E, Martens S, Tulli S. The Role of ATG9 Vesicles in Autophagosome Biogenesis.
523 Journal of Molecular Biology 2024; 436:168489.
524 21. Matoba K, Kotani T, Tsutsumi A, Tsuji T, Mori T, Noshiro D, Sugita Y, Nomura N,
525 Iwata S, Ohsumi Y, et al. Atg9 is a lipid scramblase that mediates autophagosomal membrane
526 expansion. Nat Struct Mol Biol 2020; 27:1185–93.
527 22. Cui Y, Parashar S, Zahoor M, Needham PG, Mari M, Zhu M, Chen S, Ho H-C, Reggiori
528 F, Farhan H, et al. A COPII subunit acts with an autophagy receptor to target endoplasmic
529 reticulum for degradation. Science 2019; 365:53–60.
530 23. Li Z, Huang W, Wang W. Multifaceted roles of COPII subunits in autophagy. Biochimica
531 et Biophysica Acta (BBA) - Molecular Cell Research 2020; 1867:118627.
532 24. Gui X, Yang H, Li T, Tan X, Shi P, Li M, Du F, Chen ZJ. Autophagy induction via
533 STING trafficking is a primordial function of the cGAS pathway. Nature 2019; 567:262–6.
534 25. Davis S, Wang J, Zhu M, Stahmer K, Lakshminarayan R, Ghassemian M, Jiang Y, Miller
535 EA, Ferro-Novick S. Sec24 phosphorylation regulates autophagosome abundance during nutrient
536 deprivation. eLife 2016; 5:e21167.
537 26. Brisset M, Grandin M, Bernet A, Mehlen P, Hollande F. Dependence receptors: new
538 targets for cancer therapy. EMBO Mol Med 2021; 13:e14495.
539 27. Berthenet K, Diazzi S, Jamard C, Stopa K, Dragan S, Fanfone D, Nguyen T, Al N, Virard
540 F, Meurette O, et al. Atypical contribution of caspase-3 to melanoma cancer cell motility by
541 regulation of coronin 1B activity [Internet]. 2024 [cited 2024 Oct 31]; Available from:
542 http://biorxiv.org/lookup/doi/10.1101/2024.06.27.601010
543 28. Schweichel JU, Merker HJ. The morphology of various types of cell death in prenatal
544 tissues. Teratology 1973; 7:253–66.
545 29. Marino G, Niso-Santano M, Baehrecke EH, Kroemer G. Self-consumption: the interplay
546 of autophagy and apoptosis. Nature reviews Molecular cell biology 2014; 15:81–94.
547 30. Huang Z, Zhou L, Chen Z, Nice EC, Huang C. Stress management by autophagy:
548 Implications for chemoresistance. International journal of cancer 2016; 139:23–32.
549 31. Denton D, Shravage B, Simin R, Mills K, Berry DL, Baehrecke EH, Kumar S.
550 Autophagy, not apoptosis, is essential for midgut cell death in Drosophila. Current biology : CB
551 2009; 19:1741–6.
552 32. Berry DL, Baehrecke EH. Growth arrest and autophagy are required for salivary gland
553 cell degradation in Drosophila. Cell 2007; 131:1137–48.
554 33. Liu Y, Shoji-Kawata S, Sumpter RM, Wei Y, Ginet V, Zhang L, Posner B, Tran KA,
555 Green DR, Xavier RJ, et al. Autosis is a Na+,K+-ATPase–regulated form of cell death triggered
556 by autophagy-inducing peptides, starvation, and hypoxia–ischemia. Proc Natl Acad Sci U S A
557 2013; 110:20364–71.
558 34. Button RW, Roberts SL, Willis TL, Hanemann CO, Luo S. Accumulation of
559 autophagosomes confers cytotoxicity. J Biol Chem 2017; 292:13599–614.

35. Kriel J, Loos B. The good, the bad and the autophagosome: exploring unanswered questions of autophagy-dependent cell death. Cell Death Differ 2019; 26:640–52.
36. Ge L, Zhang M, Kenny SJ, Liu D, Maeda M, Saito K, Mathur A, Xu K, Schekman R. Remodeling of ER -exit sites initiates a membrane supply pathway for autophagosome biogenesis. EMBO Reports 2017; 18:1586–603.
37. Li S, Yan R, Xu J, Zhao S, Ma X, Sun Q, Zhang M, Li Y, Liu J-JG, Chen L, et al. A new type of ERGIC–ERES membrane contact mediated by TMED9 and SEC12 is required for autophagosome biogenesis. Cell Res 2022; 32:119–38.
38. Davis S, Wang J, Zhu M, Stahmer K, Lakshminarayan R, Ghassemian M, Jiang Y, Miller EA, Ferro-Novick S. Sec24 phosphorylation regulates autophagosome abundance during nutrient deprivation. eLife 2016; 5:e21167.
39. Davis S, Wang J, Ferro-Novick S. Crosstalk between the Secretory and Autophagy Pathways Regulates Autophagosome Formation. Developmental Cell 2017; 41:23–32.
40. Jeong Y-T, Simoneschi D, Keegan S, Melville D, Adler NS, Saraf A, Florens L, Washburn MP, Cavasotto CN, Fenyö D, et al. The ULK1-FBXW5-SEC23B nexus controls autophagy. eLife 2018; 7:e42253.
41. Xun J, Zhang Z, Lv B, Lu D, Yang H, Shang G, Tan JX. A conserved ion channel function of STING mediates noncanonical autophagy and cell death. EMBO Rep 2024; 25:544–69.
42. Wu M, Zhang X, Zhang W, Chiou YS, Qian W, Liu X, Zhang M, Yan H, Li S, Li T, et al. Cancer stem cell regulated phenotypic plasticity protects metastasized cancer cells from ferroptosis. Nat Commun 2022; 13:1371.
43. Nassour J, Radford R, Correia A, Fusté JM, Schoell B, Jauch A, Shaw RJ, Karlseder J. Autophagic cell death restricts chromosomal instability during replicative crisis. Nature 2019; 565:659–63.
44. Nassour J, Aguiar LG, Correia A, Schmidt TT, Mainz L, Przetocka S, Haggblom C, Tadepalle N, Williams A, Shokhirev MN, et al. Telomere-to-mitochondria signalling by ZBP1 mediates replicative crisis. Nature 2023; 614:767–73.

Figure legends

Figure 1. The Kremen-1/DKK1 pair is altered in cancers.

(**A,B**) *Kremen1* (A) and *DKK1* (B) expression was assessed in paired Normal /Tumoral sample from different cancers from TCGA dataset BRCA: Breast invasive carcinoma; COAD: Colon adenocarcinoma; ESCA: Esophageal carcinoma; HNSC: Head and Neck squamous cell carcinoma; KIRP: Kidney renal clear cell carcinoma; PCPG: Pheochromocytoma and Paraganglioma; THCA: Thyroid carcinoma. (**C,D**) Kaplan-Meier survival analysis of *DKK1* expression (low or high) in pancreatic adenocarcinoma (**C**) and breast cancer (**D**) patients from the TCGA dataset. (**E-H**) Violin plot of *DKK1* (**E,F**) and *Kremen1* (**G,H**) expression across different subtypes of breast cancer patients from the TCGA (**E,G**) and metabric datasets (**F,H**). One-way ANOVA was performed with a Tukey's multiple comparison test (*** p-value < 0.001; **** p-value < 0.0001).

601 **Figure 2: Kremen1 does not induce apoptotic cell death**

602 (**A**) Cell death was measured by propidium iodide incorporation in MDA-MB-231 with or without
603 Kremen1 expression upon doxycycline treatment (0,5 and 2 µg/mL). Two-way ANOVA was used
604 to assess effect of concentration on cell death induction (****: p-value <0.0001). (**B**) Colony
605 formation assay using crystal violet with or without Kremen1 expression following dox treatment
606 (dox 2µg/mL) and quantification of the colonies. Student's t-test was performed to compare mean
607 of two groups. (*: p-value<0.05). (**C**) Cell death measured by propidium iodide incorporation upon
608 Kremen1 expression in presence or not of DKK1 expression and western blot analysis showing the
609 expression of Kremen1 is similar in the two cell lines. Two-way ANOVA test was used to compare
610 control and DKK1 expressing groups. (****: p-value<0.0001). (**D**) Cell death was measured by
611 propidium iodide incorporation every two hours with the incucyte after treatment with Doxycycline
612 (1µg/ml) to induce Kremen1 expression in presence or not of qVD-oph treatment (5µM). (**E**)
613 Nanolive imaging analysis comparing Kremen1 expressing cells and apoptotic cells treated with
614 BV6 (1µM). (**F**). Cell death of MDAMB231 cells 30 hours after treatment with doxycycline
615 (1µg/ml) to induce Kremen1 expression in presence or not of Ferrostatin (Fer, 10µM) or
616 necrostatin-1 (Nec, 10µM). One-way ANOVA was performed with Tukey's multiple comparison
617 test. (**: p-value<0.01).

618

619 **Figure 3: Kremen1-induced cell death displays autophagic features**

620 (**A**) Transmission electronic microscopy of MD-AMB-231 cells expressing Kremen1 showing
621 numerous vacuoles and autophagic features (white arrow). (**B**) Western blot showing LC3 and p62
622 expression upon doxycycline treatment with the indicated concentrations at 8h, 14h and 24 hours.
623 (**C**) Confocal images of MDAMB231 cells expressing the RFP-GFP-LC3 reporter treated with
624 doxycycline (Kremen1) or not (Control) for 12 hours. (**D**) Measure of cell death by propidium
625 iodide incorporation following Kremen1 expression (DOX) in presence or not of Spautin-1 (1µM)
626 (**E**) Measure of cell death by propidium iodide incorporation following Kremen1 expression
627 (DOX) in presence or not of Wortmanin (5µM). (**F-G**) Monitoring of cell death following
628 transfection with siRNA targeting ATG9A in BxPC3 cells (**F**) or MDAMB231 (**G**) followed by
629 Kremen1 induction (Dox; 1 µg/ml). (**H**) Monitoring of cell death of MDA-MB-231 cells treated
630 (Dox; 1 µg/ml) or not to induce Kremen1 following transfection with siRNA targeting ATG18B .

631 Ratio paired Student's t-test was used to test the effect of knock-down on cell death on three
632 independent experiment (*: p-value<0.05 ; **: p-value<0.01).
633

634 **Figure 4: SEC24C is implicated in Kremen1-induced cell death**

635 (**A**) Volcano plot showing protein identified by mass spectrometry in Kremen1 interactome. (**B**)
636 STRING database protein interaction network map highlighting members of the COP-II complex
637 revealed by mass spectrometry. (**C**) Confocal imaging showing cells stained with DAPI, Kremen1
638 antibody (red) or Sec24C antibody (Green) and merged on BxPC3 cell line treated with
639 doxycycline (1 µg/ml) to induce Kremen1. (**D**) Cell death induction following Kremen1 induction
640 (dox, 2µg/ml) and knock-down of SEC24C by siRNA in MDA-MB -and BxPC3 cells. Ratio paired
641 Student's t-test was used to test the effect of knock-down on cell death on three independent
642 experiment (**: p-value<0.01). (**E**) Western blot analysis of SEC24C, Kremen1, Actin and LC3
643 expression following inhibition of Sec24C by siRNA at 12h, 14h and 36h and associated
644 quantification at 24h.
645

646 **Figure 5: Kremen1 is interacting with ATG9A and SEC24C after membrane trafficking**
647 (**A**) PLA images and quantification of Kremen1/SEC24C and Kremen1/ATG9A interaction
648 following Doxycycline treatment (0,5 µg/ml) to induce Kremen1. Student's t-test was performed
649 on automated counting using Signal Image Artist software (****: p-value< 0,0001). (**B**) PLA was
650 performed after incubation of live cells with Kremen1 antibody as indicated in the scheme. PLA
651 was then performed with only SEC24C or ATG9 antibody to test proximity with internalized
652 Kremen1 (iK1). Student's t-test was performed on automated counting using Signal Image Artist
653 software (****: p-value< 0,0001).
654

655 **Figure 6: Kremen1 induces SEC24C/ATG9A/ATG8 interaction at ERGIC**
656 (**A**) Western blot analysis following immunoprecipitation of SEC24C upon Kremen1 expression
657 and associated quantification. (**B**) Confocal imaging showing cells stained with LC3 (red) SEC24C
658 (Green) or DAPI following Kremen1 induction. (**C**) PLA images and quantification of
659 LC3/SEC24C, LC3/ATG9A and LC3/ERGIC (LMAN1) interaction in presence of Kremen1

660 induction Student's t-test was performed on automated counting using Signal Image Artist software
661 (****: p-value< 0,0001).
662
663
664

Brahim, Schott et al., Figure 1

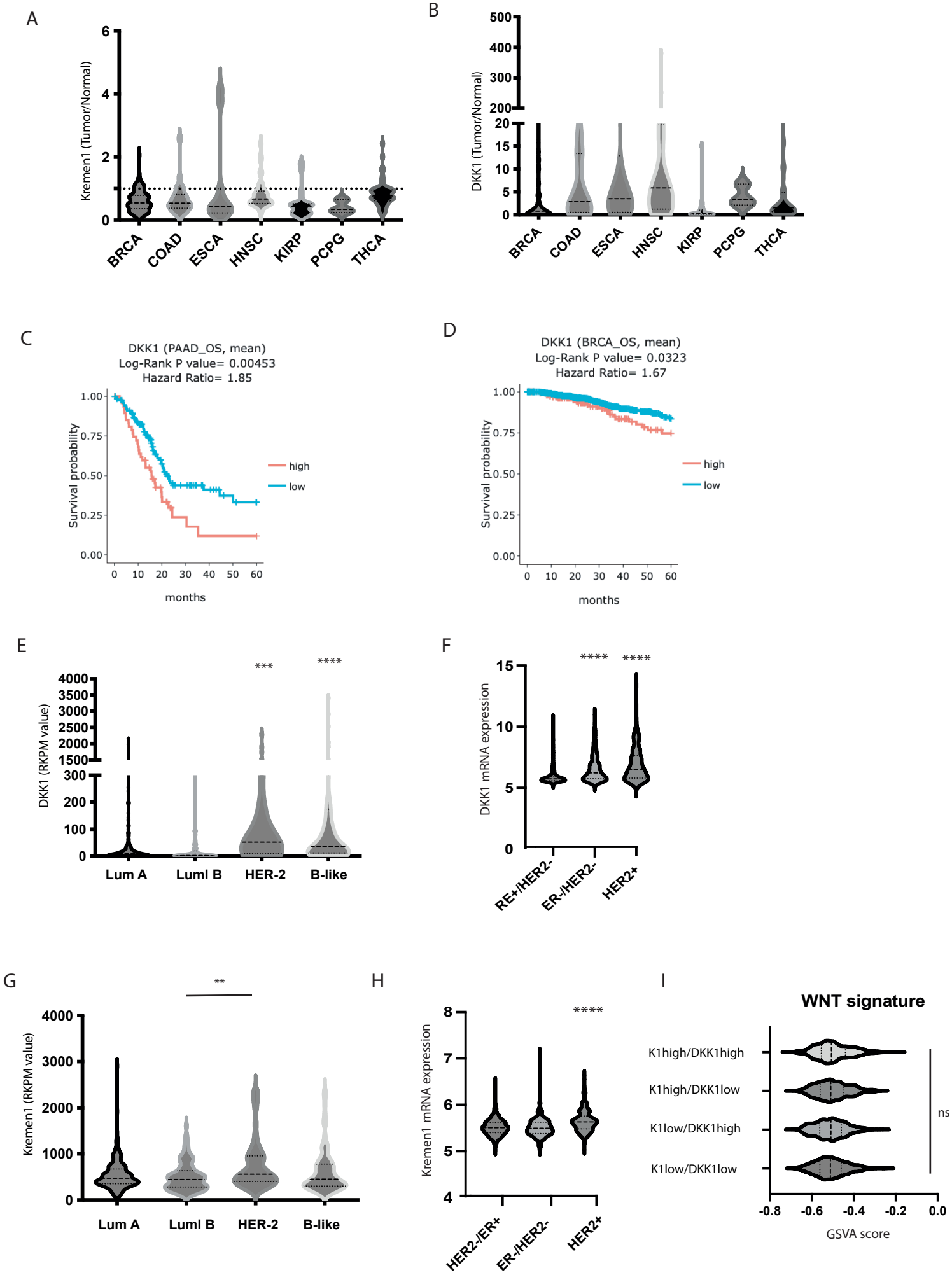

Brahim, Schott et al., Figure 2

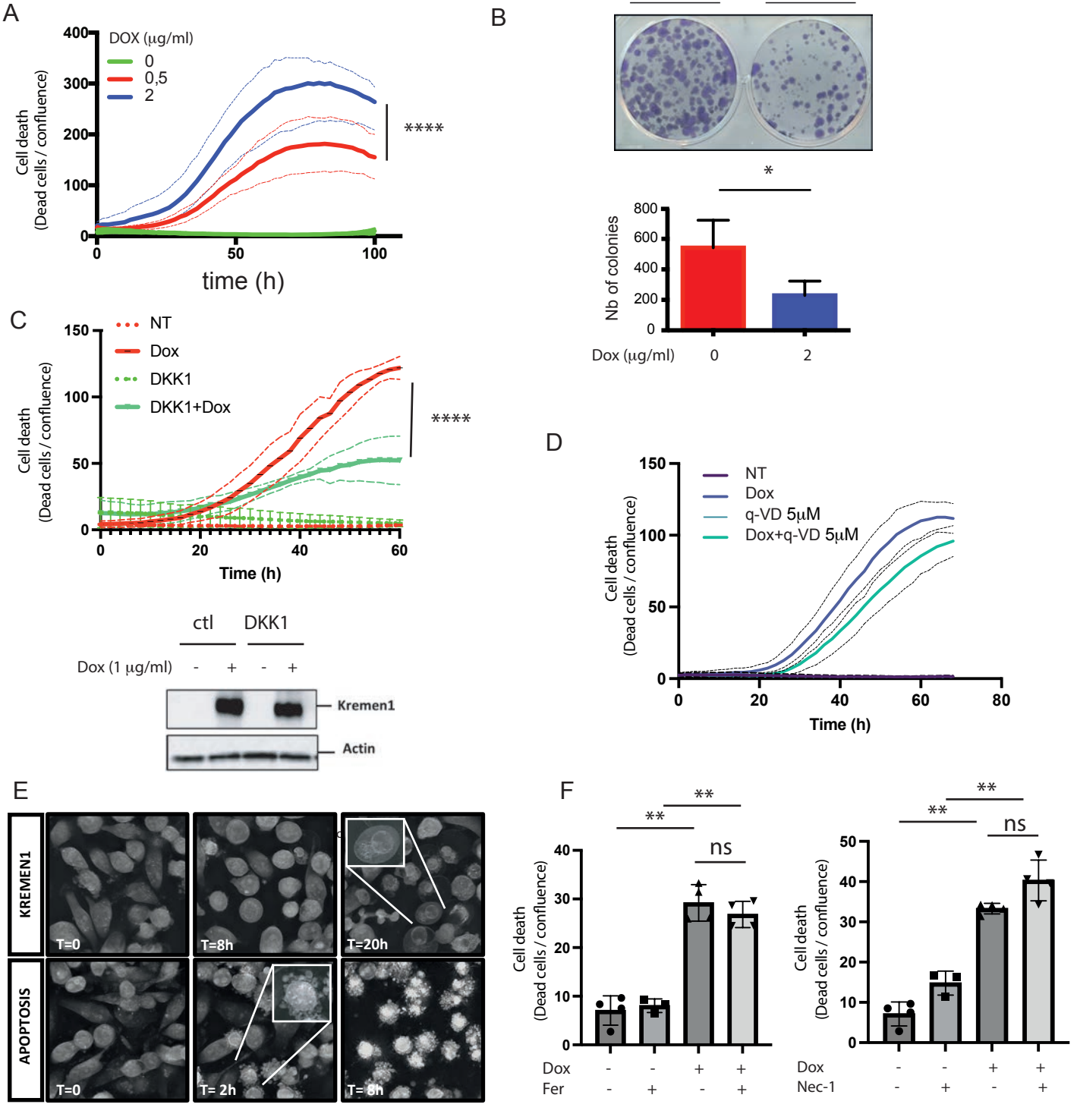

Brahim, Schott et al., Figure 3

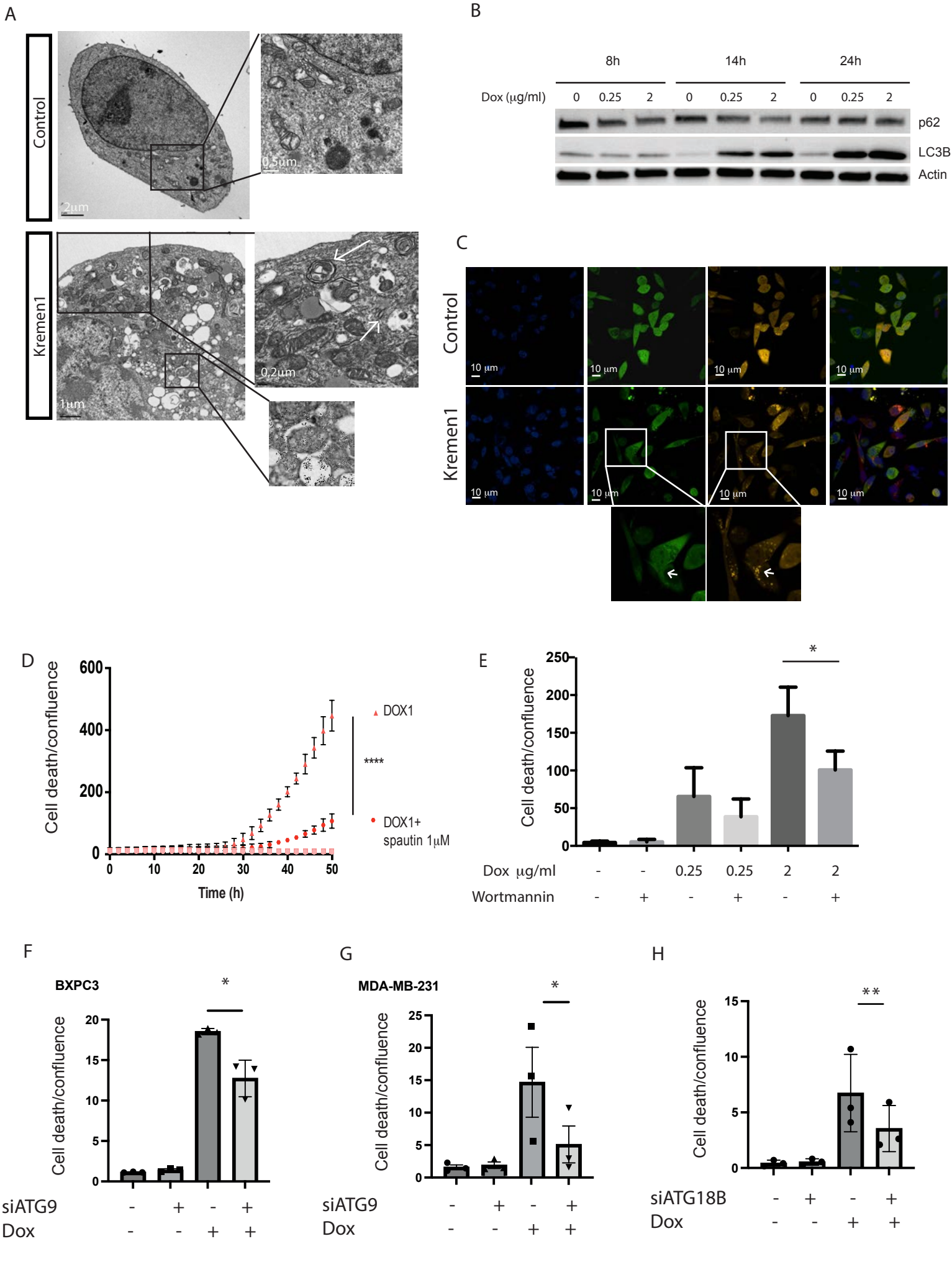

Brahim, Schott et al., Figure 4

A

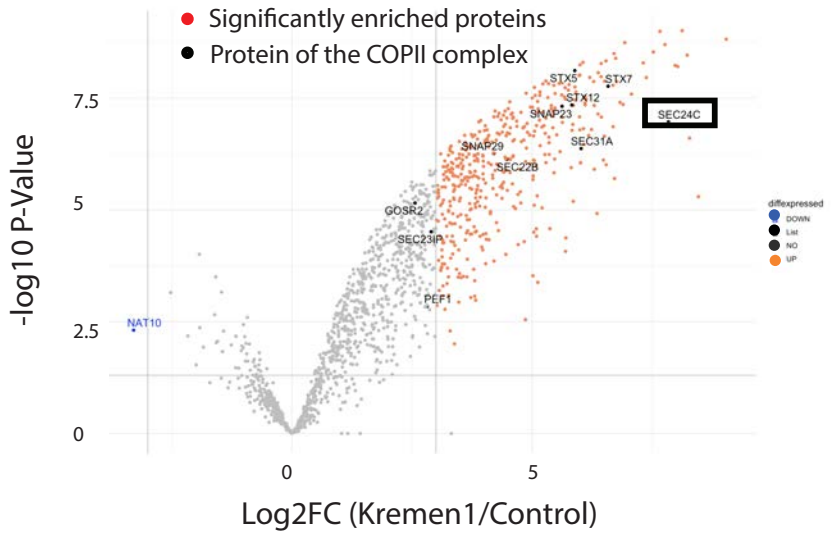

B

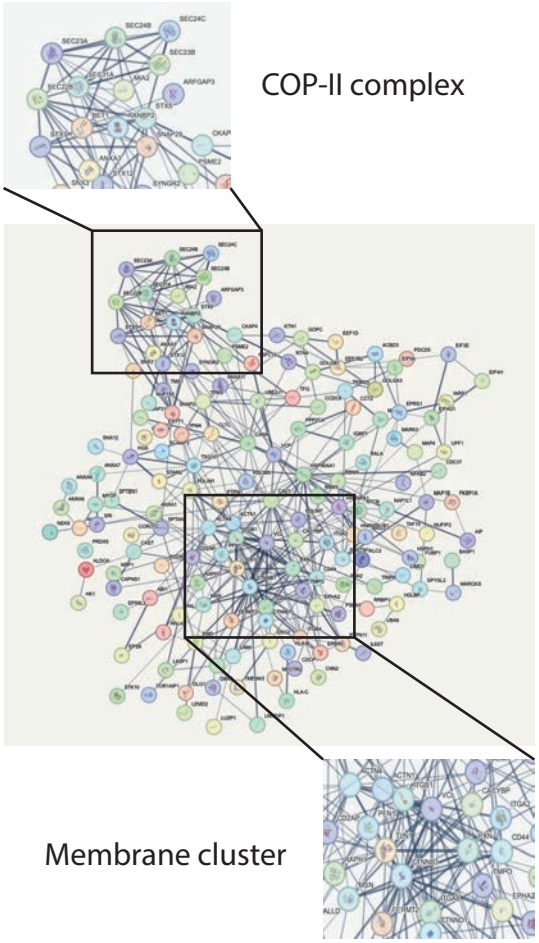

C

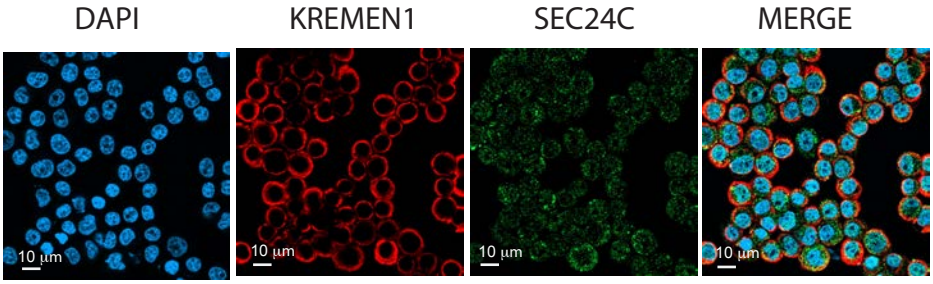

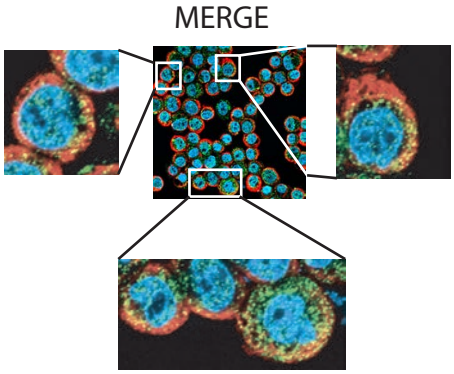

D

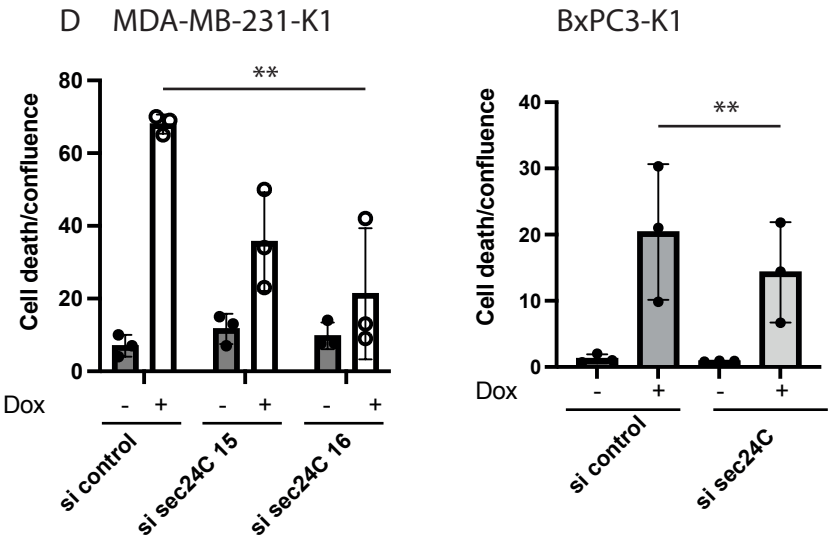

E

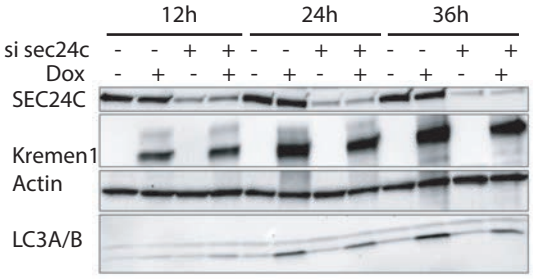

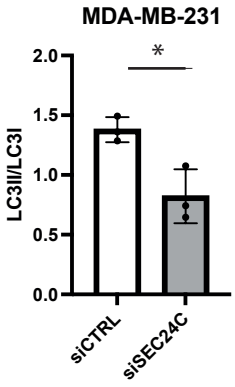

Brahim, Schott et al., Figure 5

A

K1 total

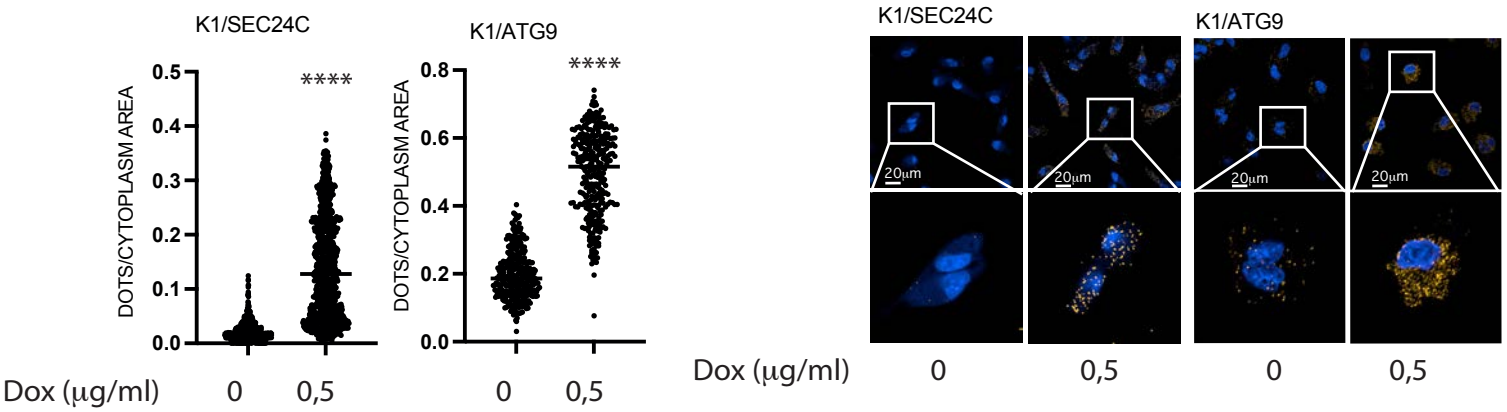

B

Internalized K1 (iK1)

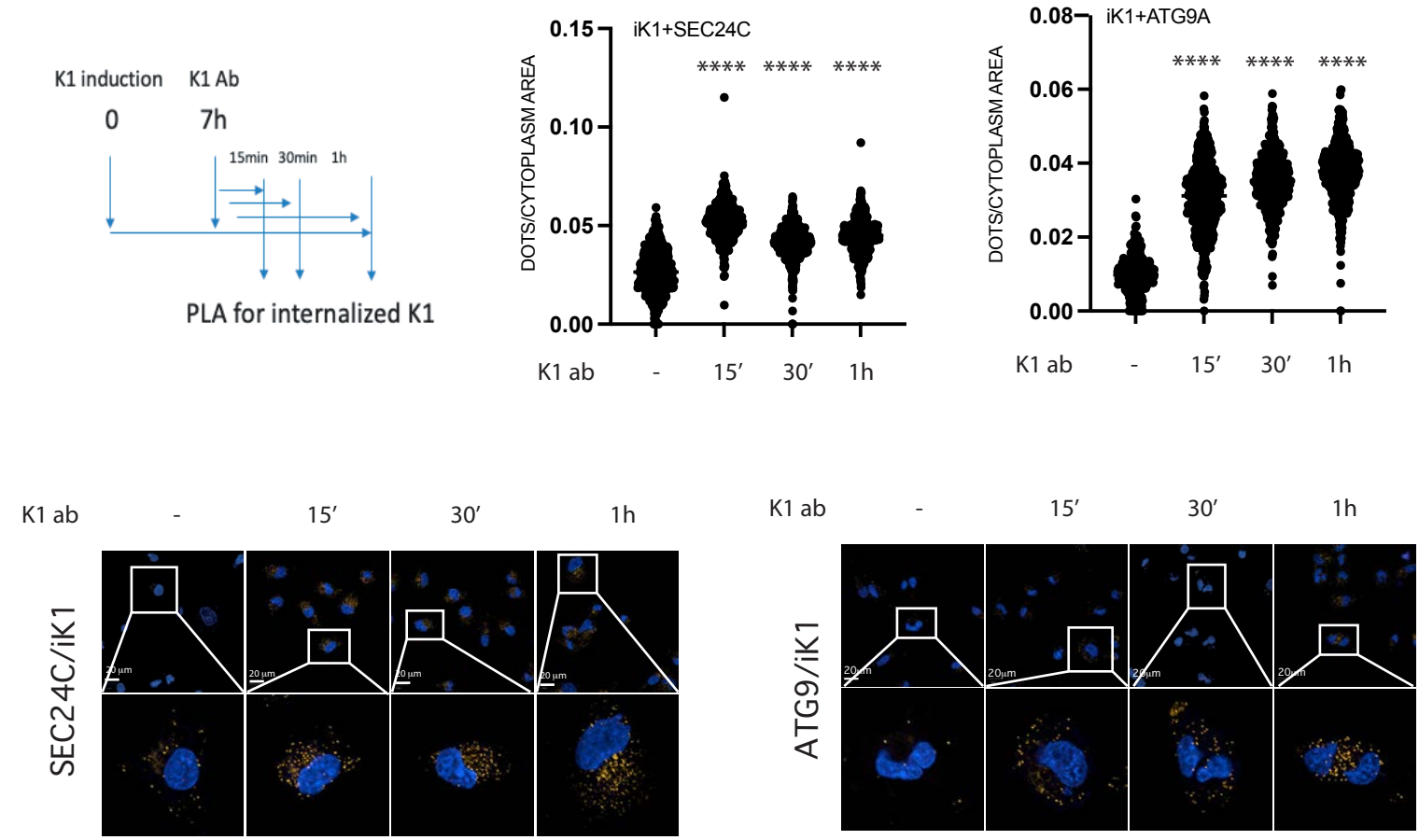

Brahim, Schott et al., Figure 6

A

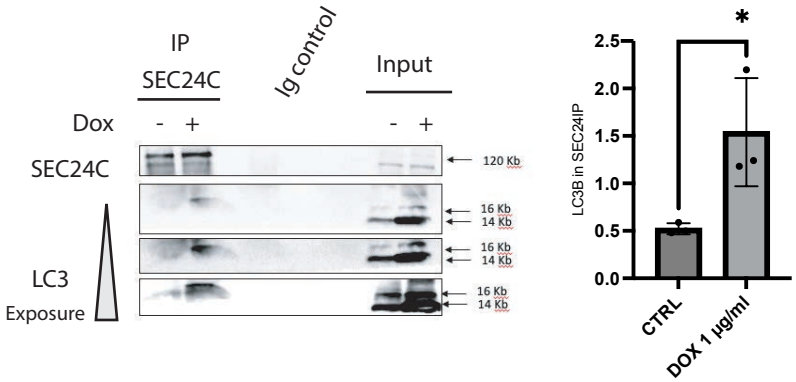

B

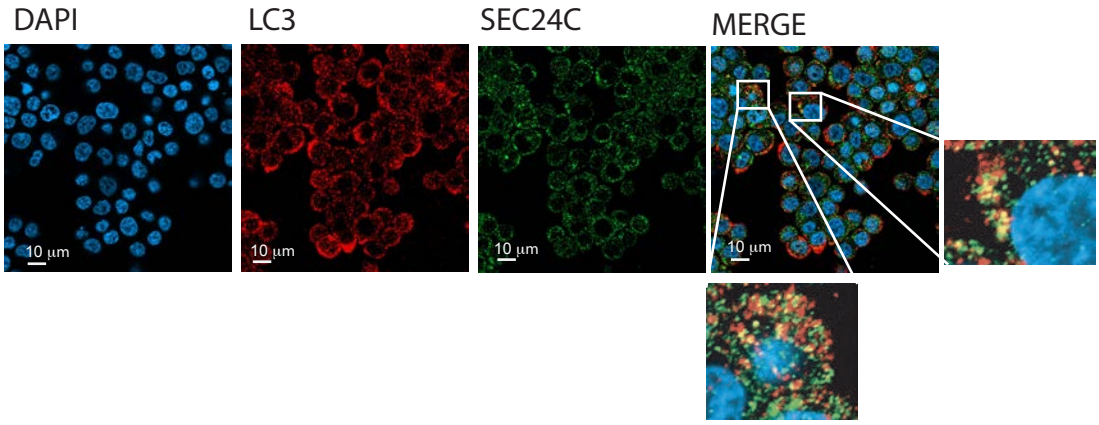
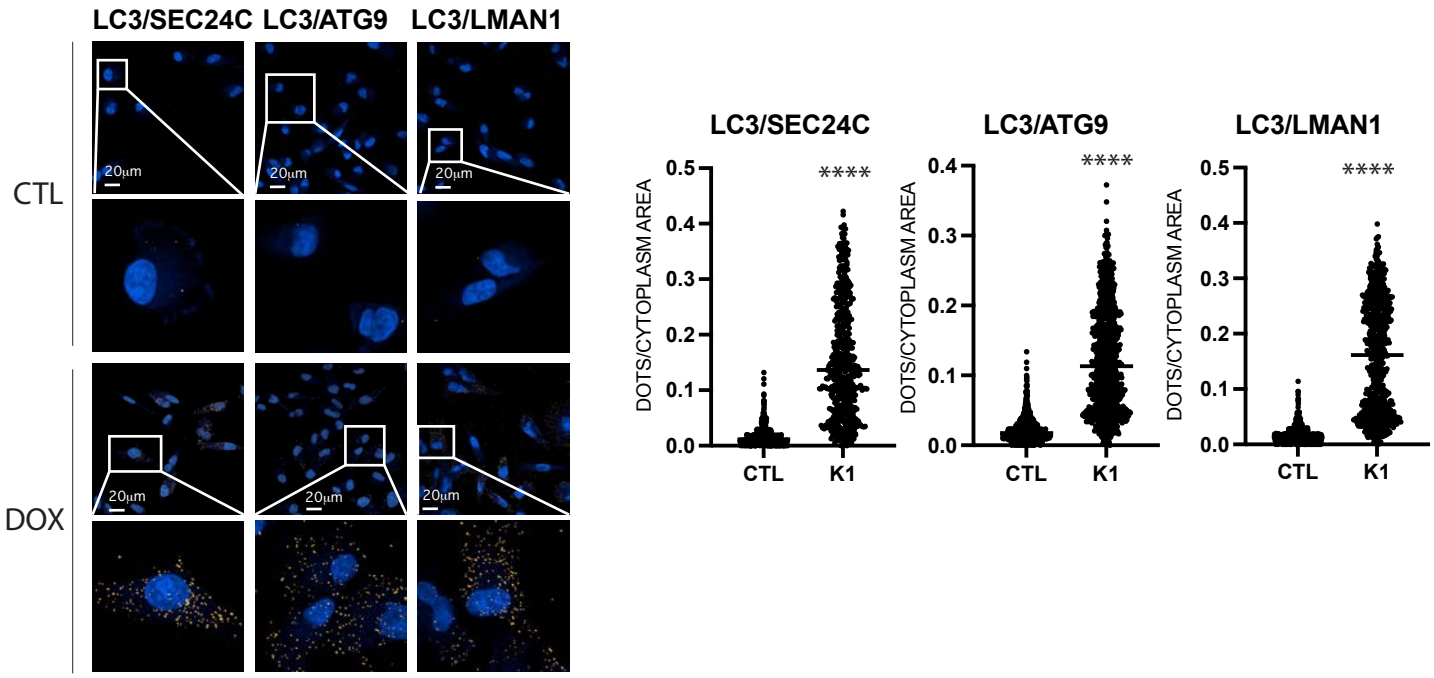
C